CHAPTER 2

Effect of PQT-12 Interface Layer on the Performance of PCDTBT:$PC_{61}BM$ Bulk Heterojunction Organic Solar Cells

Contents

*Part of this work has been published as:

Amit Kumar et al., "Effect of PQT-12 interface layer on the performance of PCDTBT:PCBM bulk heterojunction solar cells," *Material Research Express*, vol. 6, no. 11, 115514, 2019.

CHAPTER 2

Effect of PQT-12 Interface Layer on the Performance of PCDTBT:$PC_{61}BM$ Bulk Heterojunction Organic Solar Cells

2.1 Introduction

Importance of the solar cell in context of green energy harvesting has already been discussed in detail in Chapter-1. Organic solar cells (OSCs) have drawn considerable attention from researchers in the last few years due to their lightweight, environment-friendly nature, fabrication possibility on flexible substrates, high throughput, and potentiality of cost-effective, fast roll-to-roll (R2R) production [93], [94]. Among the various organic solar cell (OSC) structures, bulk heterojunction (BHJ) OSC is a promising solar cell technology having the general structure of (ITO or FTO coated glass substrate)/ETL/Active layer/HTL/Metallic electrode shows the better capability for superior performance. It has opened up several design aspects such as controlling the photoactive layer's morphology, interface layer insertion, and feasibility of multilayer deposition through the solution process, etc. [26], [93], [95]–[100].

In the recent few years, among various donor-acceptor polymers, poly[N-9′-hep-tadecanyl-2,7-carbazole-alt-5,5-(4′,7′-di-2-thienyl-2′,1′,3′-benzothiadiazole)] (PCDTBT): Phenyl-C_{61}-butyric acid methyl ester ($PC_{61}BM$) [58], [61], [76]–[79] has shown considerable interest as the active material in the BHJ OSCs. The large bandgap metal oxides (e.g. ZnO, TiO_2 etc.) are widely used for the electron trnasport layer (ETL) [65]. Among them, ZnO is the most commonly used metal oxide for the electron transport layer (ETL) [71], [72] in OSCs.

Because, ZnO has a large bandgap energy which is suitable for complete absorption of the UV light. Further, it has a good level allignment property with the $PC_{61}BM$ which allows only the transporation of electrons while blocking the transportation of holes. Moreover, ZnO can be easily synthesized by low-cost solution process which enables to fabricate low-cost BHJ OPVs. The non-toxic environ-friendly nature of the ZnO also makes it a favorable for electronic and optoelectronic applications. In general, various nanostructures of the ZnO are used for the ETL [65], [71], [72]. However, colloidal ZnO quantum dots (QDs) based ETL layer has not been explored in the BHJ OPVs. It is interesting to note that the energy bandgap of the ZnO QDs can be tuned by tuning the sizes of the QDs [101]. Therefore, we have explored the colloidal ZnO QDs for the ETL in the BHJ OPV considered in this chapter.

PEDOT: PSS is extensively used for the hole transport layer (HTL) [102] [103], [104]. However, direct deposition of PEDOT:PSS on the active layer may degrade the quality of the underneath active material and hence the performance of the BHJ OSCs [100], [104]. The poly (3, 3’’’- dialkylquaterthiophene) (PQT-12) may be used as an interfacial layer in between the HTL and active layer due to its good phase matching and energy band alignment with the active layer to achieve improved charge transport in the device [105]–[108]. The floating-film transfer method (FTM), originally proposed by Morita et al. [109] and later optimized by others [110]–[113], is a relatively new cost-effective thin film deposition technique for obtaining thin PQT-12 films [114] in organic devices.

The present chapter investigates the effect of FTM based PQT-12 film on the performance of ZnO quantum dots (QDs)/PCDTBT:$PC_{\mathbf{61}}BM$/PQT-12/ PEDOT:PSS based

OSCs where the layer of ZnO QDs acts as the ETL, PCDTBT:$PC_{61}BM$/ acts as the active layer, PQT-12 film acts as an interfacial layer (IL) and PEDOT: PSS layer acts the HTL in the device. The ZnO QDs are synthesized by the low cost-cost solution method. The performance parameters of the BHJ OSCs with and without the PQT-12 IL have been compared. The outline of the rest of this chapter is as follows:

Section 2.2 exhibits the experimental details of the fabrication of PCDTBT:$PC_{61}BM$ BHJ OSC. The results and discussion related to the electrical and optical characterizations of the fabricated device have been included in Section 2.3. Finally, Section 2.4 concludes the objectives and outcomes of the research carried out in this chapter.

2.2 Experimental Details

2.2.1 Materials and Synthesis

The polymer PCDTBT was purchased from Sigma-Aldrich (India), $PC_{61}BM$ and PEDOT:PSS were purchased from Ossila (United Kingdom), and PQT-12 was purchased from American Dye Source (Canada). All the other chemicals were purchased from Merck Chemicals (India). The colloidal ZnO QDs were synthesized from zinc acetate dehydrate as a precursor illustrated in Figure 2.1. It was dissolved in 2-methoxyethanol (as coordinate ligand) under flow of nitrogen gas in a three-neck flask and then equivalent molar of monoethanolamine (MEA) was added as a reagent for stabilization purpose using the technique described in [101]. The prepared colloidal ZnO QDs solution was then stirred for 24 h in an inert atmosphere. Finally, the resulting solution was filtered using a polyvinylidene fluoride (PVDF) membrane (0.22 μm) to obtain ZnO QDs of uniform size by discarding the unreacted particles [101].

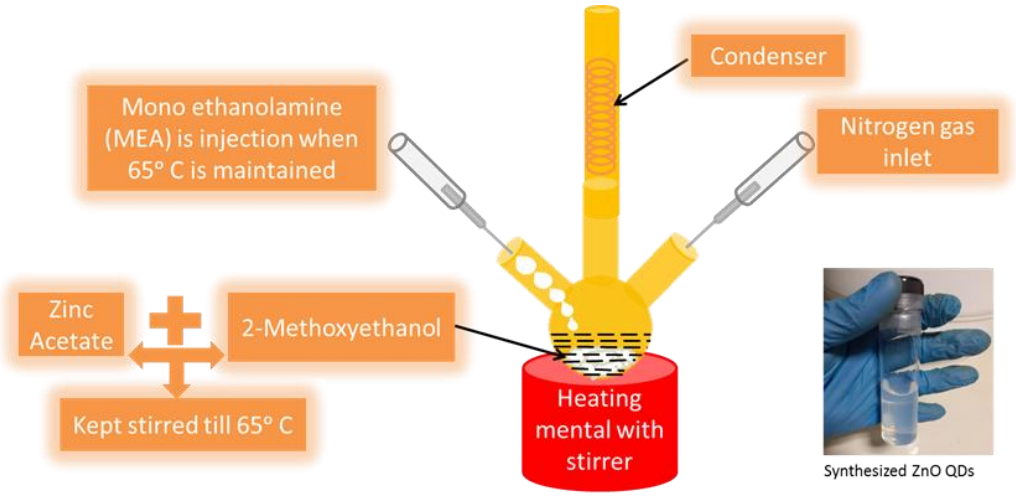

Figure 2.1: Synthesis process of ZnO QDs.

2.2.2 Device Fabrication

The BHJ OSC devices were fabricated on ITO coated soda-lime glass substrate in an ambient air atmosphere unless and otherwise specific conditions are mentioned. The fabrication of the OSCs was started with the cleaning of ITO-coated glass substrates (15×15 mm^2) for all types of devices. The ITO-coated glass substrates were cleaned ultrasonically in a soap solution, deionized (DI) water, acetone, and isopropanol for 10 minutes, sequentially. The substrates were dried at 100°C in the oven under nitrogen gas flow for 15 minutes. The synthesized ZnO QDs solution of 100 mM was deposited on ITO film by the spin coating technique at 2000 rpm for 40 s. The film was dried at 110°C for 10 minutes, and then the spin coating was repeated for one more time. Finally, the film was annealed at 200°C in an ambient air atmosphere for 30 minutes to achieve a ~30 nm thickness of ZnO QDs to work efficiently as the ETL of BHJ OSC. For the deposition of the active layer, a blend solution of PCDTBT (5 mg/ml in dichlorobenzene) and $PC_{61}BM$

(15 mg/ml in chloroform) was prepared by stirring overnight. The blend solution was deposited on the ZnO QDs layer by spin coating technique at 1500 rpm for 40 s and then dried at 120°C in the oven under a nitrogen environment for 30 min.

Two types of devices were fabricated: "Device 1" used the ITO/ZnO QDs/PCDTBT:$PC_{61}BM$/PEDOT:PSS/Ag structure and "Device 2" used a PQT-12 IL to form the structure of ITO/ZnO QDs/PCDTBT:$PC_{61}BM$/PQT-12/PEDOT:PSS/Ag under study. The PEDOT:PSS HTL was deposited by the conventional spin coating at 2000 rpm for 40 s and dried it at 120°C for 30 min to obtain a thickness of ~40 nm. The PQT-12 was deposited using the FTM technique, as illustrated in Figure 2.2 [110] [112]. It should be noted that the PQT-12 was dissolved in chloroform (a non-polar solvent), and this hydrophobic solution was dispersed on the hydrophilic (ethylene glycol and glycerol in 1:1 ratio) liquid (liquid substrate). Also, the surface of the active layer (a blend of PCDTBT and $PC_{61}BM$) was of hydrophobic nature. Thus, the surface of the active layer (hydrophobic) promotes adhesion for PQT-12 during film stamping using the FTM technique and thus offers a better interface [112], [114]. The PQT-12 film of ~20 nm was obtained over the active layer and was then dried at 120°C for 10 min in a nitrogen environment. Finally, a 100 nm thin Ag metal electrode of 2 mm diameter was deposited by a thermal evaporation method (Model no. FL400 SMART COAT 3.0 A from Hind High Vacuum) using shadow masking technique at a vacuum level of ~3×10^{-6} mbar and a constant rate of 0.2 Å/s. The complete device structures of the BHJ OSCs are shown in Figure. 2.3.

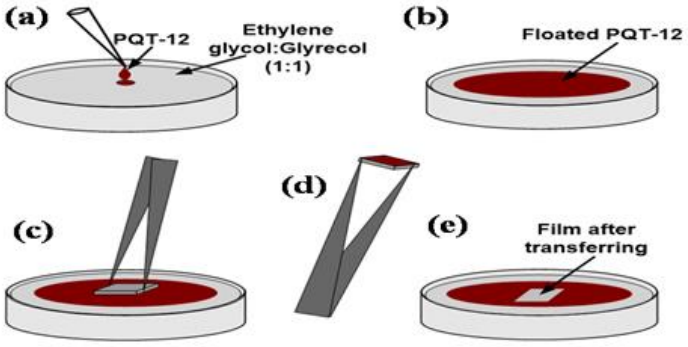

Figure 2.2: The schematic diagram of floating film transfer method (a) Dropping of PQT-12 on the hydrophilic solution (ethylene glycol and glycerol in 1:1 ratio), (b) Thin film of PQT-12 over the liquid surface, (c) Transferring of the film on the substrate, (d) PQT-12 coated substrate and (e) Empty space in PQT-12 film in the liquid surface.

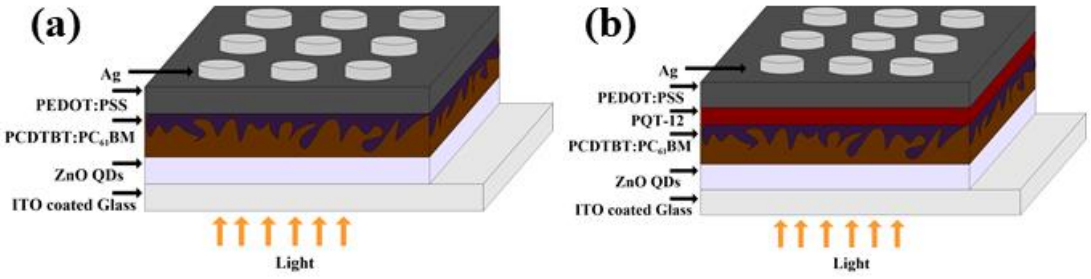

Figure 2.3: Device structure of fabricated OSCs (a) Device 1 and (b) Device 2.

2.3 Results and Discussion

In this section, thin-film and electrical as well as optical characterization of the PCDTBT:$PC_{61}BM$ based BHJ organic solar cell have been carried out.

2.3.1 Thin Film Characterization

The optical absorbance of the thin films was measured by UV/Vis/NIR spectroscopy (Model V-750 from Jesco, Japan). The photoluminescence (PL) from various thin-film

structures is measured by using a spectrometer (FLS 980 from Edinburgh Instruments, UK). The electrical characterization (current density vs. voltage, J-V) was carried out by using a semiconductor parameter analyzer (Model B1500A from Keysight, USA). The standard solar spectrum was obtained from a solar simulator (Model SS50AAA, A.M. 1.5G from Photo Emission Technology Inc., USA). The power density (light intensity) of the obtained solar spectrum is calibrated using a standard silicon reference cell (Model 60623 provided by Photo Emission Technology Inc., USA). The external quantum efficiency (EQE) was calculated with the help of a discrete spectrum obtained from a halogen lamp with the help of a monochromator (Model SP2150i from Princeton Instruments, USA).

The energy band diagram for both the OSCs structures fabricated using blend film of PCDTBT:$PC_{61}BM$ are shown in Figure 2.4. In Device 1, PEDOT:PSS as HTL blocks the electron and transports the hole, as shown in Figure 2.4 (a). In Device 2, the insertion of the PQT-12 IL between the active layer and PEDOT:PSS enhance hole transportation with a good energy band alignment, as shown in Figure 2.4 (b). Since the PEDOT:PSS is not in direct contact with the active layer, the insertion of PQT-12 IL also enhances the stability of the BHJ OSC under study. The absorption spectra of the ZnO/ PCDTBT:$PC_{61}BM$ and ZnO/PCDTBT:$PC_{61}BM$/PQT-12 films are shown in Figure 2.5. The solar spectrum of energy higher than 1.8 eV is absorbed by PCDTBT:$PC_{61}BM$ polymer blend. However, due to the thin film of the active layer (~80 nm), a significant part of the solar spectrum with energy higher than 1.8 eV is transmitted to PQT-12. The absorption spectra shown in Figure 2.5 illustrate that the use of FTM coated PQT-12 as the IL enhances the absorption in the active layer of the device. The charge extraction from the active layer

(PCDTBT:$PC_{61}BM$) at the interface is investigated using steady-state photoluminescence measurements [115]. The measurements for three film structures ZnO/PCDTBT:$PC_{61}BM$, ZnO/ PCDTBT:$PC_{61}BM$/PEDOT:PSS,and ZnO/PCDTBT:$PC_{61}BM$/PQT-12/PEDOT:PSS respectively are performed from glass side at an excitation wavelength of 540 nm as shown in the Figure. 2.6. It is found that the PEDOT:PSS only HTL quenched PL intensity slightly due to transfer of hole from the active layer to PEDOT:PSS. This PL intensity quenching further increases in the ZnO/ PCDTBT:$PC_{61}BM$/PQT-12/PEDOT:PSS film structures due to insertion of PQT-12 IL results in more efficient charge transfer at the interface (also seen from band diagram of Figure 2.4).

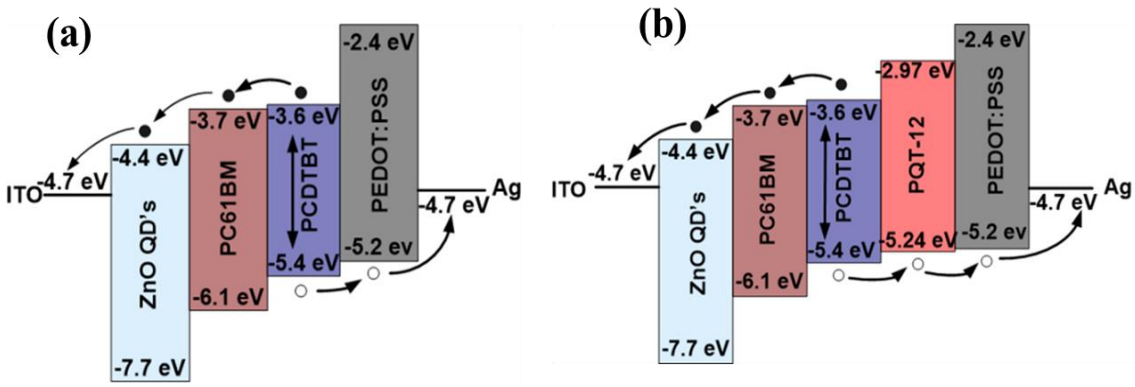

Figure 2.4: Energy band diagram of (a) Device 1 and (b) Device 2.

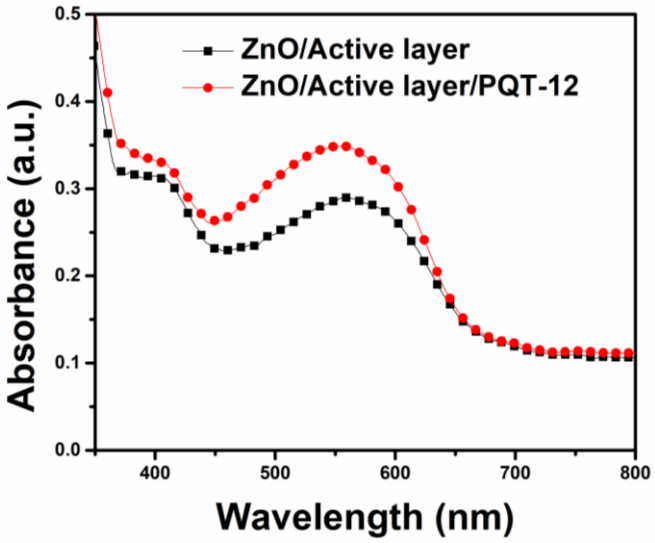

Figure 2.5: Absorption spectra of ZnO/Active layer and ZnO/Active layer/PQT-12 films.

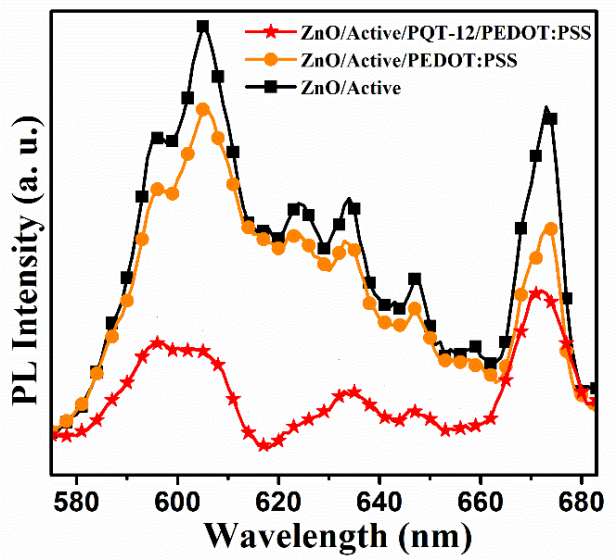

Figure 2.6: Photoluminescence (PL) spectra of ZnO/Active, ZnO/Active/PEDOT:PSS, and ZnO/Active/PQT-12/PEDOT:PSS films taken from glass side at an excitation of 540 nm.

2.3.2 Solar Cell Characterization

The *J-V* characteristics shown in Figure 2.7 are measured under illuminated conditions for both the BHJ OSCs under study. The non-ideal or S-shape J-V characteristics in the

figure are attributed to the rectifying contact between the hole collecting electrode and PEDOT:PSS layer resulted from the increased sheet resistance of the PEDOT:PSS based HTL [116]. It is believe that the PEDOT:PSS layer near the electrode contact gets dissolved in water and increases the sheet resistance of the PEDOT:PSS layer. Another possible reason behind the non-ideal or S-shape J-V curves is the reduced surface recombination velocity at the electrode/HTL interface [117]. The performance parameters of the BHJ OSCs are summarized in Table 2.1. The better power conversion, as well as other parameters in Device 2 over Device 1 listed in Table 2.1, are attributed to the FTM-based PQT-12 film as IL in the device. The maximum power conversion efficiency of 1.05% achieved in Device 2 attributed to the improved hole transfer and enhanced optical absorption, as observed in Figure 2.5. The best results for the open-circuit voltage (V_{OC}), short circuit current density (J_{SC}), and fill factor (FF) of 0.562 V, 5.62 mA/cm^2, and 0.33, respectively, are also obtained in Device 2. The V_{OC} closely depends on the difference of HOMO of electron donor polymer and LUMO of electron acceptor polymer [118]. According to Shockley's formula, the current density of the diode (heterostructure) is expressed as:

$$J = J_0[\exp(qV/nkT) - 1] \tag{2.1}$$

Where J_0 is reverse saturation current density, *k* is the Boltzmann constant, *T* is temperature, and *n* is the ideality factor of the diode. Including the effects of series resistance (R_S) and shunt resistance (R_{sh}), equation 2.1 can be modified as equation. 2.2 [40]:

$$J = \frac{Rsh+Rs}{Rsh}\left\{J_0\left[\left(\exp\frac{q(V-JRs)}{nKT}\right) - 1\right] + \frac{V}{Rsh}\right\} - J_{ph} \tag{2.2}$$

Using $V = V_{OC}$ and J=0 in the equation. 2.2 and assuming $R_{sh} >> R_s$, the open-circuit voltage

V_{OC} can be written as:

$$V_{OC} = \frac{nkT}{q} ln\left(\frac{J_{ph}}{J_0} + 1\right) \quad (2.3)$$

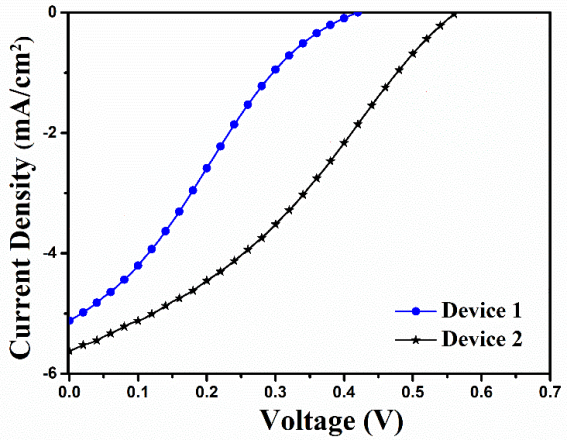

Figure 2.7: Current density versus voltage (J-V) characteristic of the fabricated OSCs.

Table 2.1: Performance parameters of the OSC devices

Device structure	V_{oc} (mV)	J_{sc} (mA/cm^2)	Fill factor (FF)	Efficiency η (%)
Device 1	419	5.12	0.24	0.53
Device 2	562	5.62	0.33	1.05

Table 2.2: Reverse saturation current of the OSC devices

Device structure	Voc (mV)	J_0 (A/cm^2)
Device 1	419	7.87×10^{-5}
Device 2	562	1.74×10^{-5}

The reverse saturation current density J_0 in equation 2.3 has been extracted from the measured J-V characteristics by following the method described in [119], [120]. The

obtained values of J_0 are in good agreement with equation 2.3 and V_{OC} calculated under the illumination of 1 sunlight. The values of J_0 are listed in Table 2.2 and compared with the corresponding V_{OC}. The barrier between HTL and the electrode, as shown in the band diagram of Figure 2.4, also supports the dark current characteristics.

The external quantum efficiency (EQE) of both devices has been shown in Figure 2.8. The enhancement in EQE in Device 2 over Device 1 is a result of improved absorption and better energy band alignment due to the insertion of the PQT-12 IL. The improved band alignment reduces the recombination and enhances the EQE by improving the transportation of selective charge carriers toward their respective electrodes (i.e., electrons toward ITO and holes toward Ag) in the BHJ OSCs.

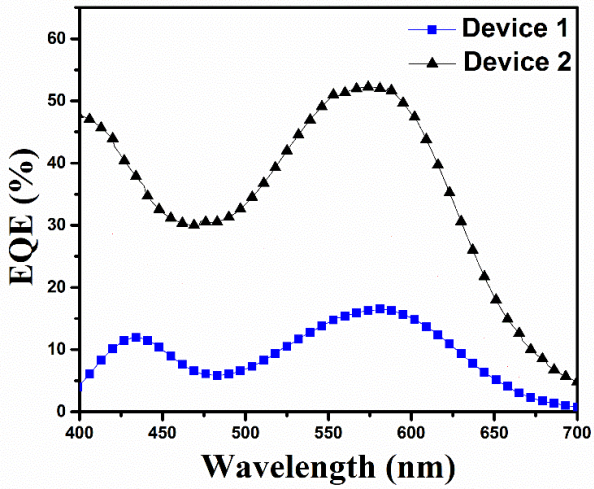

Figure 2.8: External quantum efficiency of the fabricated OSCs.

The impedance spectroscopy is performed for the measurement of resistance and capacitance associated with OSCs equivalent circuit. The impedance spectroscopy analysis of our OSCs is performed by using the Nyquist plot where x-axis represents the real (Z_1) and y-axis shows the imaginary (Z_2) part of the impedances. The frequency is varied in

such a way that it is decreased with the increase in the distance from the origin. The Nyquist plots (Cole-Cole plots) of the fabricated OSCs under dark condition are shown in Figure 2.9 (a) at an applied bias corresponding to their respective open circuit voltages, V_{OC}. Figure 2.9 (a) shows the semicircle which corresponds to the parrelel RC circuit shown in Figure 2.9 (b). The parallel resistance R_2 in the RC circuit represents the diameter of the semicircle which corresponds to the bulk resistance. On the other hand, C_2 in the RC circuit corresponds to the simple geometrical capacitance of the device [121]. Cole-Cole plots or Nyquist plots of the fabricated OSCs under dark condition are shown in Figure 2.9 (a) at an applied bias corresponding to their V_{OC}. The data obtained from Nyquist plots can be modeled for an equivalent circuit, as shown in Figure 2.9 (b). The resistance R_1 in series with the parallel combination of the resistance R_2 and capacitor C_2 is due to the resistive losses and interface mismatch [121]. The higher value of resistance R_1 is observed in Device 1, whereas lower R_1 is observed in Device 2. This reduction in the value of R_1 in Device 2 is due to better phase matching of the active layer with FTM-based PQT-12 as IL compared to that without IL between the active layer and PEDOT:PSS. The smallest semicircle for Device 2 in the Nyquist plot confirms the best charge transportation due to its lowest resistance value R_1. Further, Device 2 is illuminated with the light of 1 sun and the corresponding Nyquist plot is shown in Figure 2.9 (c). Under the illumination of light, two partial semicircles are formed as visible from Figure 2.9 (c). Therefore, a relatively more complex equivalent circuit model as shown in Figure 2.9 (d) is required to fit the solar cell impedance characteristic under illumination condition [121]. The second part ($R_3\|C_3$) of the equivalent circuit observed by the second semicircle is due to the generation/recombination of charge carriers and charge transfer at the interfaces.

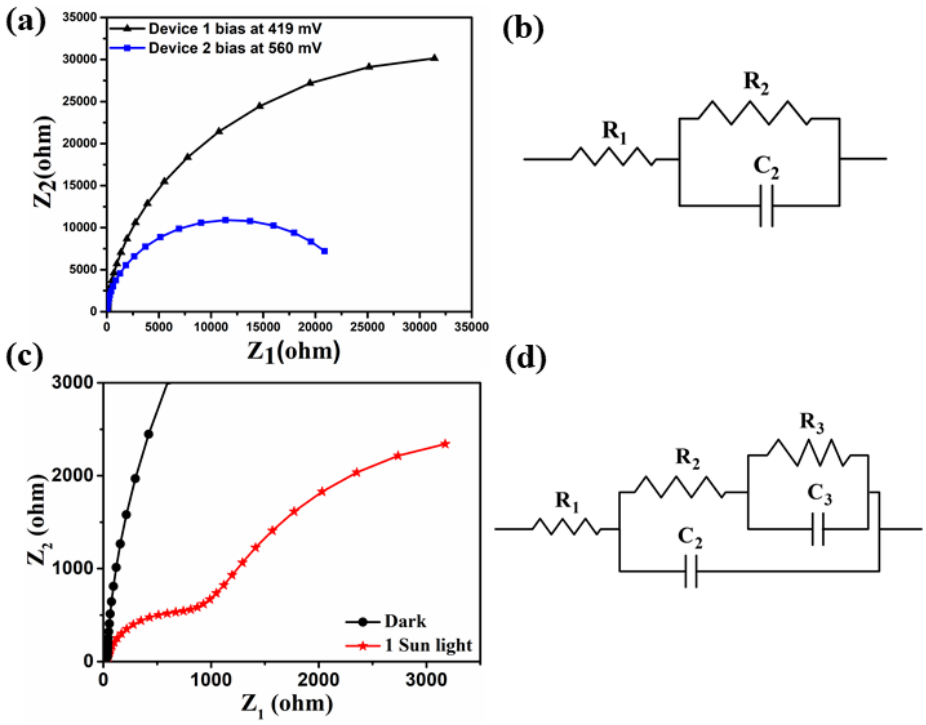

Figure 2.9: (a) Nyquist plot of the fabricated OSCs under dark condition, (b) Equivalent circuit of the OSCs under dark, (c) Nyquist plot of Device 2 under dark and light illumination, and (d) Equivalent circuit of the Device 2 under dark and light illumination.

2.4 Conclusion

In this chapter, the incorporation of FTM-based PQT-12 as an interface layer between the active layer and HTL shows better performance and stability. Well-matched HOMO level of PQT-12 (5.24 eV) and PEDOT:PSS (5.2 eV) with that of PCDTBT (5.4 eV) donor material have been used to facilitate better hole transportation to Ag electrode. The maximum values of J_{SC} (= 5.62 mA/cm^2), V_{OC} (= 562 mV), FF (= 0.33), and PCE (= 1.05%) have been measured in the OSC with PQT-12 as IL. The efficient hole transfer from the active layer to the electrode also enhanced the EQE to the maximum when PQT-

12 IL layer is inserted between the active layer and PEDOT:PSS. The impedance spectroscopy analysis is performed for the modelling of BHJ OSCs to obtain a simplified equivalent circuit of the OSCs under study. The FTM based PQT-12 as IL shows significant PL quenching and improves absorbance in the active layer, which, in turn, improves the PCE.

CHAPTER 3

Effects of HTL and ETL Thicknesses on the Performance of PQT-12/PCDTBT:$PC_{61}BM$/ZnO QDs Organic Solar Cells

Contents

*Part of this work has been published as:

Amit Kumar et al., "Effects of HTL and ETL Thicknesses on the Performance of PQT-12/PCDTBT:$PC_{61}BM$/ZnO QDs Solar Cells," *IEEE Photonics Technology Letters*,32 (12), 677-680, 2020.